# Organic Tribotronic Transistor for Contact-Electrification-Gated Light-Emitting Diode

*Chi Zhang, Jing Li, Chang Bao Han, Li Min Zhang, Xiang Yu Chen, Li Duo Wang, Gui Fang Dong,* and Zhong Lin Wang**

**Tribotronics is a new field about the devices fabricated using the electrostatic potential created by contact electrification as a "gate" voltage to tune/control charge carrier transport in semiconductors. In this paper, an organic tribotronic transistor is proposed by coupling an organic thin film transistor (OTFT) and a triboelectric nanogenerator (TENG) in vertical contact-separation mode. Instead of using the traditional gate voltage for controlling, the charge carrier transportation in the OTFT can be modulated by the contact-induced electrostatic potential of the TENG. By further coupling with an organic light-emitting diode, a contact-electrification-gated light-emitting diode (CG-LED) is fabricated, in which the operating current and light-emission intensity can be tuned/controlled by an external force–induced contact electrification. Two different modes of the CG-LED have been demonstrated and the brightness can be decreased and increased by the applied physical contact, respectively. Different from the conventional organic light-emitting transistor controlled by an electrical signal, the CG-LED has realized the direct interaction between the external environment/stimuli and the electroluminescence device. By introducing optoelectronics into tribotronics, the CG-LED has open up a new field of tribophototronics with many potential applications in interactive display, mechanical imaging, micro-opto-electro-mechanical systems, and flexible/touch optoelectronics.**

## 1. Introduction

Organic light-emitting transistors (OLETs) are a new type of optoelectronic devices, which combine the electrical switching functionality of organic thin film transistors (OTFTs) and the light emission of organic light-emitting diodes (OLEDs) in a single device.[1,2] OLETs have potential applications in optical communication systems,[3] panel display technology,[4] solid-state lighting,[5] and electrically pumped organic lasers.[6] As the OLETs have a structure of three terminals, an externally supplied gate voltage is needed for modulating the light-emission intensity, which lacks the direct interaction mechanism between the external environment and optoelectronic devices. Based on the piezoelectric-semiconductor materials such as ZnO and GaN, strain-enhanced LEDs have been developed by using the strain-induced piezopotential to control the carrier recombination and improve the light-emission intensity.[7–10] The strain-enhanced LEDs coupled piezoelectric, semiconductor, and optoelectronic properties are the typical representatives in an emerging field of piezophototronics,[11,12] which was first proposed in 2010 after the introduction of piezotronics in 2007.[13,14]

Recently, the invention of the triboelectric nanogenerator (TENG) has provided an effective approach to convert ambient mechanical energy into electricity,[15–19] which has great application in not only micro-energy,[20,21] macro-energy,[22,23] and active sensors,[24,25] but also tribo-controlled devices.[26–28] Tribotronics is a new field about the devices fabricated using the electrostatic potential created by triboelectrification as a "gate" voltage to tune/control charge carrier transport in semiconductors.[29,30] Without the limitation to the piezoelectric semiconductor materials, tribotronics can be extended to organic materials for the interactive application with the organic semiconductor devices.

Here in this work, we developed an organic tribotronic transistor (OTT) by coupling an OTFT and a TENG in vertical contact-separation mode, in which the charge carrier transportation in the OTFT can be modulated by the contact-induced electrostatic potential instead of the traditional gate voltage. By further coupling with an OLED, a contact-electrification-gated light-emitting diode (CG-LED) was developed for demonstrating the tribo-controlled light-emission characteristics. With the direct interaction between the external environment and the electroluminescence device, the CG-LED has potential applications in interactive display, mechanical imaging, micro-opto-electro-mechanical systems, and flexible/touch optoelectronics.

Dr. C. Zhang, Dr. C. B. Han, L. M. Zhang, Dr. X. Y. Chen, Prof. Z. L. Wang
Beijing Institute of Nanoenergy and Nanosystems
Chinese Academy of Sciences
Beijing 100083, P.R. China
J. Li, Prof. L. D. Wang, Prof. G. F. Dong
Chemistry Department
Tsinghua University
Beijing 100084, P.R. China
E-mail: donggf@mail.tsinghua.edu.cn
Prof. Z. L. Wang
School of Material Science and Engineering
Georgia Institute of Technology
Atlanta, GA 30332-0245, USA
E-mail: zlwang@gatech.edu

**DOI: 10.1002/adfm.201502450**

## 2. Principles and Characteristics

### 2.1. Structure of the CG-LED

The basic structure of the CG-LED is composed of an OLED, an OTFT, and a TENG in vertical contact-separation mode, as schematically illustrated in **Figure 1**a. The OTFT is prepared on a glass substrate with an indium tin oxide (ITO) layer of 180 nm thick as the gate electrode.[31,32] A $Ta_2O_5$ film as gate dielectric is prepared by magnetron sputtering with a thickness of about 275 nm. Then a pentacene film is deposited by thermal evaporation with a thickness of about 65 nm. Finally, the drain/source electrodes, 55 nm thick Au films, are deposited on two sides of the pentacene film with Ohmic contacts. The channel length is 60 μm and the width is 1000 μm. A Cu film of the TENG is deposited on the bottom of the OTFT and the mobile layer is assembled next to the fixed Cu film, which consists of a piece of polyvinylchloride (PVC) film with a Cu electrode deposited on the back side. It can vertically contact with and separate from the fixed Cu film by an external force. The two Cu electrodes of the TENG are electrically connected to the ITO gate electrode and Au source electrode, respectively, and the OTFT and TENG have combined into the OTT as a new tribotronic device. The OLED is also prepared on a glass substrate with an ITO layer of 180 nm thick as the anode. An *N*,*N*′-diphenyl-*N*,*N*′-bis(1,1′-biphenyl)-4,4′-diamine (NPB) film and a tris-(8-hydroxyquinoline) aluminum ($Alq_3$) film are deposited in sequence on the ITO layer by vacuum deposition, with a total thickness of 330 nm. The NPB film is used as the hole-transporting layer and the $Alq_3$ film is used as the electron conduction and light-emitting layer. Then an Mg–Ag alloy film with deposition ratio of 10:1 is fabricated on the organic layers and an Ag film is finally formed. The Mg:Ag/Ag layers are used as the cathode with a total thickness of 65 nm. The OLED is linked on top of the OTT by a glass film and the light can be emitted up through the transparent ITO glass with an emission area of 3 mm × 3 mm.

In the CG-LED, the OTT and OLED are electrically connected in series with a voltage source. The equivalent circuit of the CG-LED can be described as shown in Figure 1b. For the OTT, the TENG can provide a gate voltage to the OTFT by applying a physical contact for controlling the drain current, which is also used for driving the OLED. Therefore, the light-emission intensity of the CG-LED can be modulated by the external force–induced contact electrification. The SEM images of the OLED in partial cross-sectional view and the OTFT in partial cross-sectional and top view are shown in Figure 1c–e, respectively.

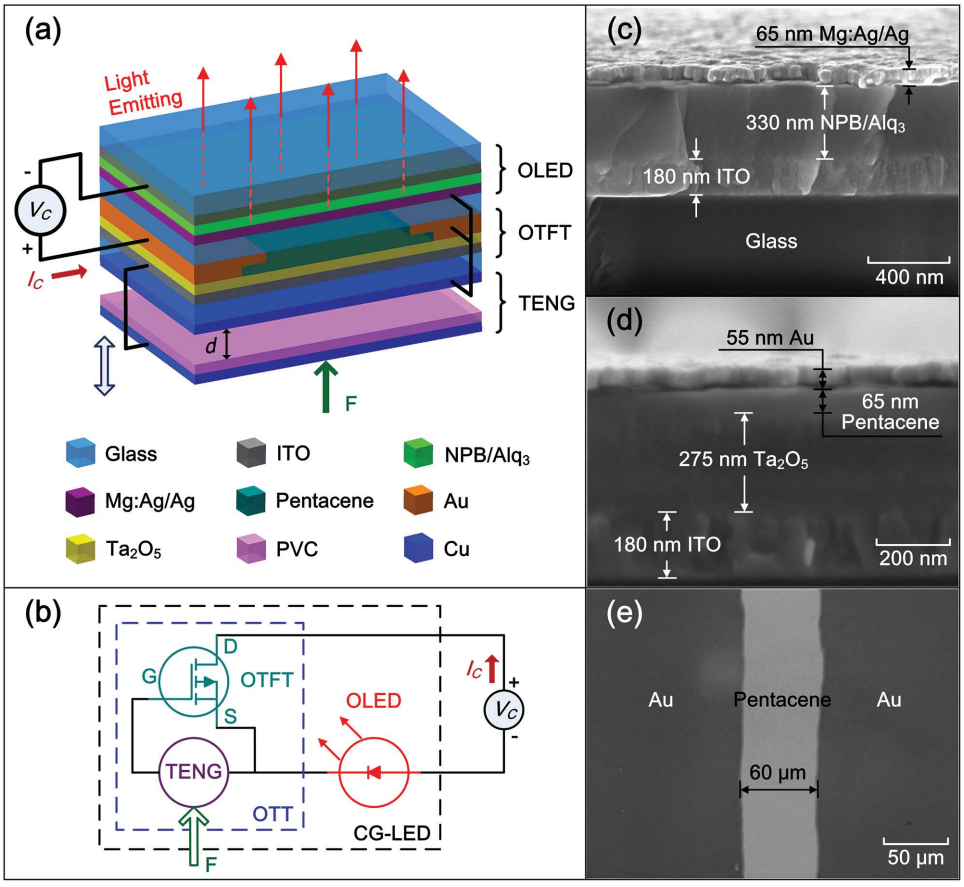


**Figure 1.** Schematic illustration of the contact-electrification-gated light-emitting diode (CG-LED). a) Structure of the CG-LED based on an organic light-emitting diode (OLED), an organic thin film transistor (OTFT), and a triboelectric nanogenerator (TENG) in vertical contact-separation mode. b) Equivalent circuit of the CG-LED. c) Partial cross-sectional view of the OLED. d) Partial cross-sectional view of the OTFT. e) Partial top view of the OTFT.

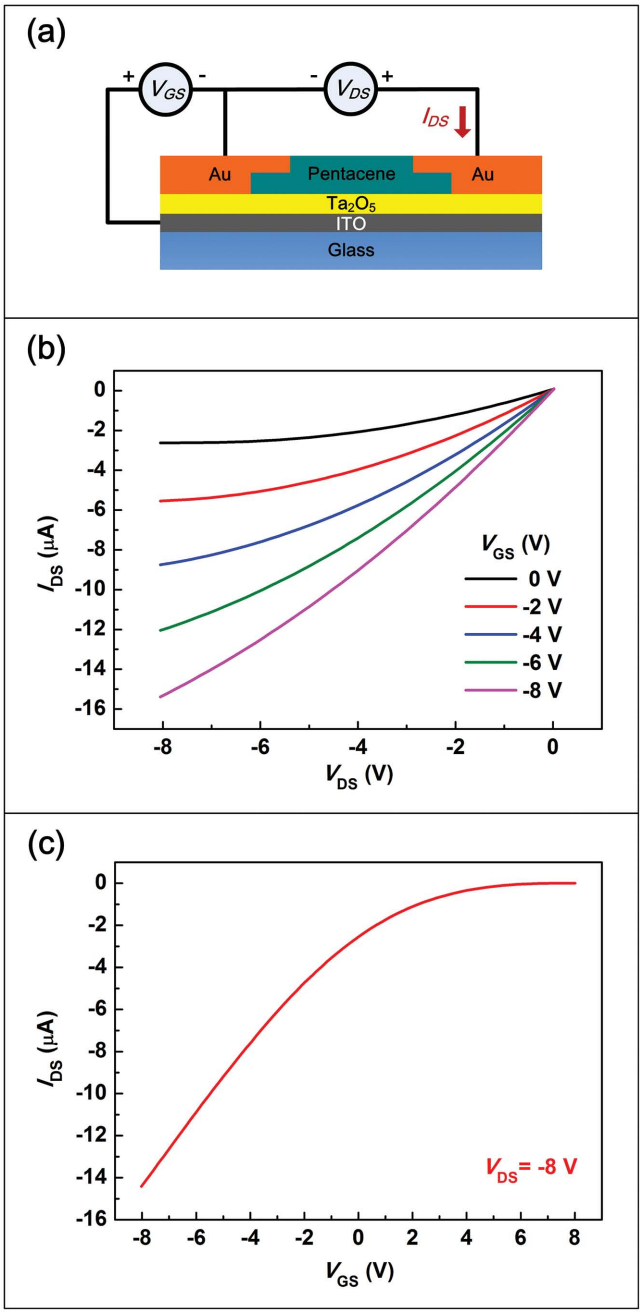


**Figure 2.** Characteristics of the OTFT. a) Schematic diagram of the OTFT on an ITO glass substrate. $Ta_2O_5$ is used as gate dielectric, pentacene as organic semiconductor, ITO as gate, and Au as source/drain top contacts. b) $I_{DS}$–$V_{DS}$ output characteristics with different $V_{GS}$. c) $I_{DS}$–$V_{GS}$ transfer characteristics at a drain voltage of –8 V.

### 2.2. Characteristics of the OTFT

The characteristics of the OTFT are measured first by applying an external gate voltage, which is schematically illustrated in **Figure 2**a. Figure 2b shows the $I_{DS}$–$V_{DS}$ output characteristics with different $V_{GS}$ from 0 to –8 V, and Figure 2c shows the $I_{DS}$–$V_{GS}$ transfer characteristics at a drain voltage of –8 V. The measured results are similar to the classical p-channel enhancement-mode MOSFET behavior in the linear and saturation regimes, which indicate that the reverse drain current is increased with the decreasing gate voltage. When the gate voltage decreases from 0 to –8 V, the p-type conduction channel in the pentacene film is broadened and the reverse drain current can be significantly modulated from 2.5 to 14.4 μA with nearly linear relationship.

### 2.3. Principle and Characteristics of the OTT

The working principle of the OTT is based on the coupling effects of the OTFT and the TENG with vertical contact-separation mode, which is schematically shown in **Figure 3**a. When the external force is applied on the mobile layer, the PVC and Cu films are vertically contacted with each other for electrification, leaving net positive charges on the fixed Cu film and net negative charges on the PVC film for the triboelectrification. The produced triboelectric charges with opposite polarities are fully balanced and the gate voltage is zero at this moment. When the external force is released, the mobile layer is separated from the fixed Cu film for a certain distance. The negative charges on the PVC film induce the electrons flow from the mobile Cu electrode to the ITO gate electrode to screen the electrostatic field. Due to the source electrode is connected to the fixed Cu film with positive charges, a negative gate voltage is applied on the OTFT and the p-type conduction channel can be broadened, which will increase the drain current. When the external force is applied and the mobile layer contacts with the fixed Cu film again, the balance of the triboelectric charges cause the electrons flow back from the ITO gate electrode to the mobile Cu electrode. The gate voltage turns back to zero and the conduction channel is narrowed, which will decrease the drain current to the original state. Therefore, the drain current of the OTT can be gated by the external force–induced contact electrification, by modulating the gap distance $d$ between the mobile layer and the fixed Cu film, which has the same effect as the traditional gate voltage. Therefore, the gap distance is used as a controlling parameter as in our following discussions.

The OTT is fixed in a precise positioning system and the gap distance $d$ can be well-controlled by the external force. Figure 3b shows the $I_{DS}$–$V_{DS}$ characteristics of the OTT with different gap distances $d$ from 0 to 800 μm, and Figure 3c shows the $I_{DS}$–$d$ transfer characteristics of the OTT at a drain voltage of –8 V. The experimental results indicate that the drain current is increased with the increasing distance, which is in accordance with the working principle in Figure 3a. At a drain voltage of –8 V, the reverse drain current is almost linearly increased from 1.9 to 12.7 μA with the increasing distance from 0 to 800 μm. As the applied gate voltage on the OTFT is negative and linearly proportional to the gap distance in this process, the OTT has the similar transfer characteristics with the OTFT and the external physical contact applied on the OTT has successfully replaced the traditional gate voltage for controlling the drain current. Based on the OTFT and TENG, the OTT has been first realized as a new tribotronic device only with metal and organic functional materials, which has demonstrated the material variety for tribotronics other than the previous silicon-based devices.[29,30]

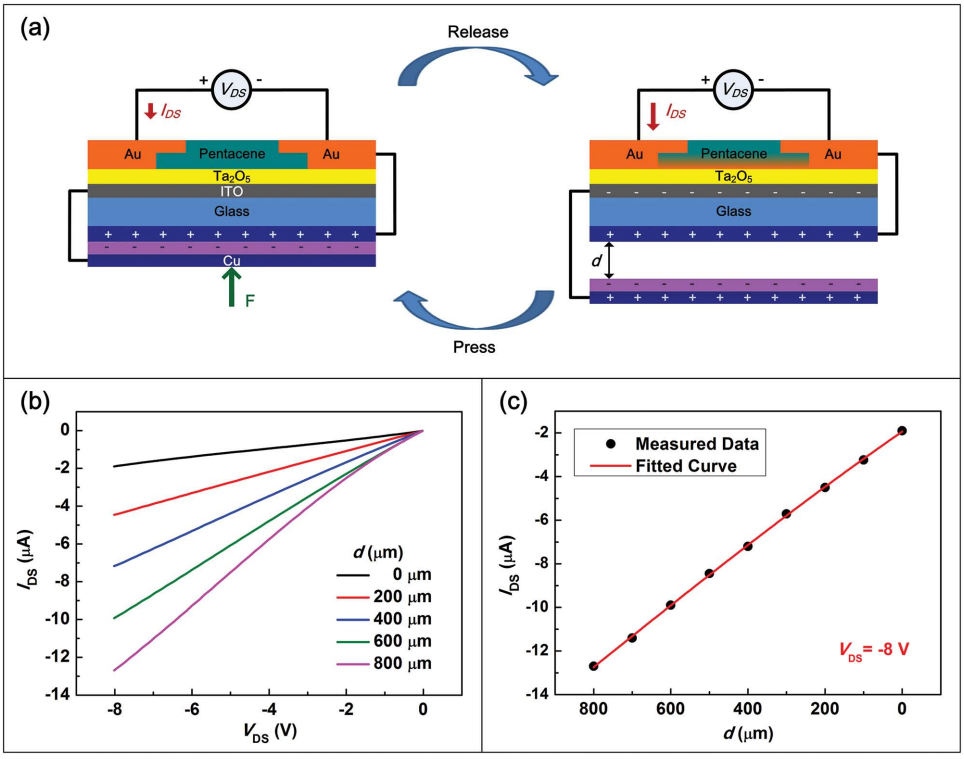


**Figure 3.** Principle and characteristics of the organic tribotronic transistor (OTT) based on the OTFT and the TENG. a) Change of the channel width and drain current when the external force is applied and released to demonstrate the working principle. b) $I_{DS}$–$V_{DS}$ characteristics of the OTT with different gap distances between the two frictional layers of the TENG. c) $I_{DS}$–$d$ transfer characteristics of the OTT at a drain voltage of –8 V.

### 2.4. Characteristics of the OLED

The characteristics of the OLED are measured independently by applying a voltage source, which is schematically illustrated in the inset of **Figure 4**a. Figure 4a shows the OLED current density and brightness are both increased with the increasing driving voltage. The OLED can brighten up faintly at 2.4 V driving voltage with 1.0 μA (0.11 A $m^{-2}$) working current, and obviously visible at 2.7 V with 12.8 μA (1.42 A $m^{-2}$). When the driving voltage is above 4 V, the current density and brightness are both increased rapidly. Figure 4b shows the emission spectra of the OLED at different driving voltages, which indicate that the light-emission intensity increases with the increasing driving voltage. The emission center near 517 nm is identified as green light emission within the emission range from 465 to 675 nm, which does not show any obvious shift when the driving voltage is changed. The OLED has demonstrated an excellent performance with low working current, which is in the modulation range of the drain current in the OTT.

### 2.5. Principles and Characteristics of the CG-LED

The working principle of the CG-LED is schematically illustrated in **Figure 5**a, in which the OTT and OLED are electrically

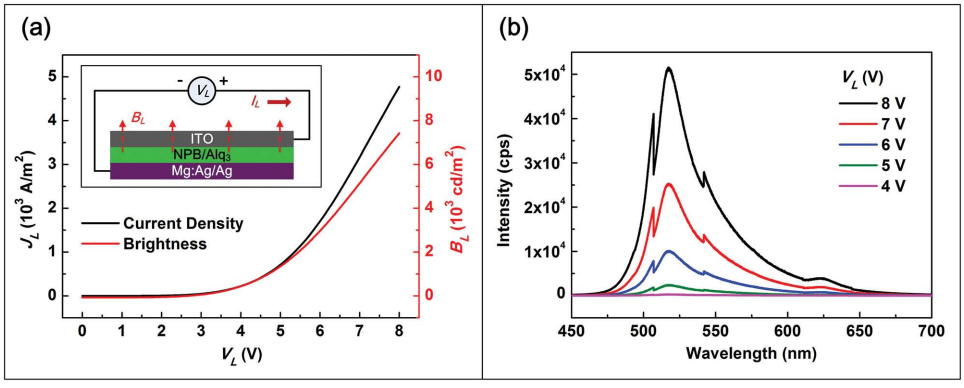


**Figure 4.** Characteristics of the OLED. a) Current and brightness versus driving voltage. The inset is the schematic diagram of the OLED. Mg–Ag alloy and Ag are used as cathode, $Alq_3$ as electron conduction and light emitting layer, NPB as hole-transporting layer, and ITO as anode. b) Optical spectrums of the OLED at different driving voltages.

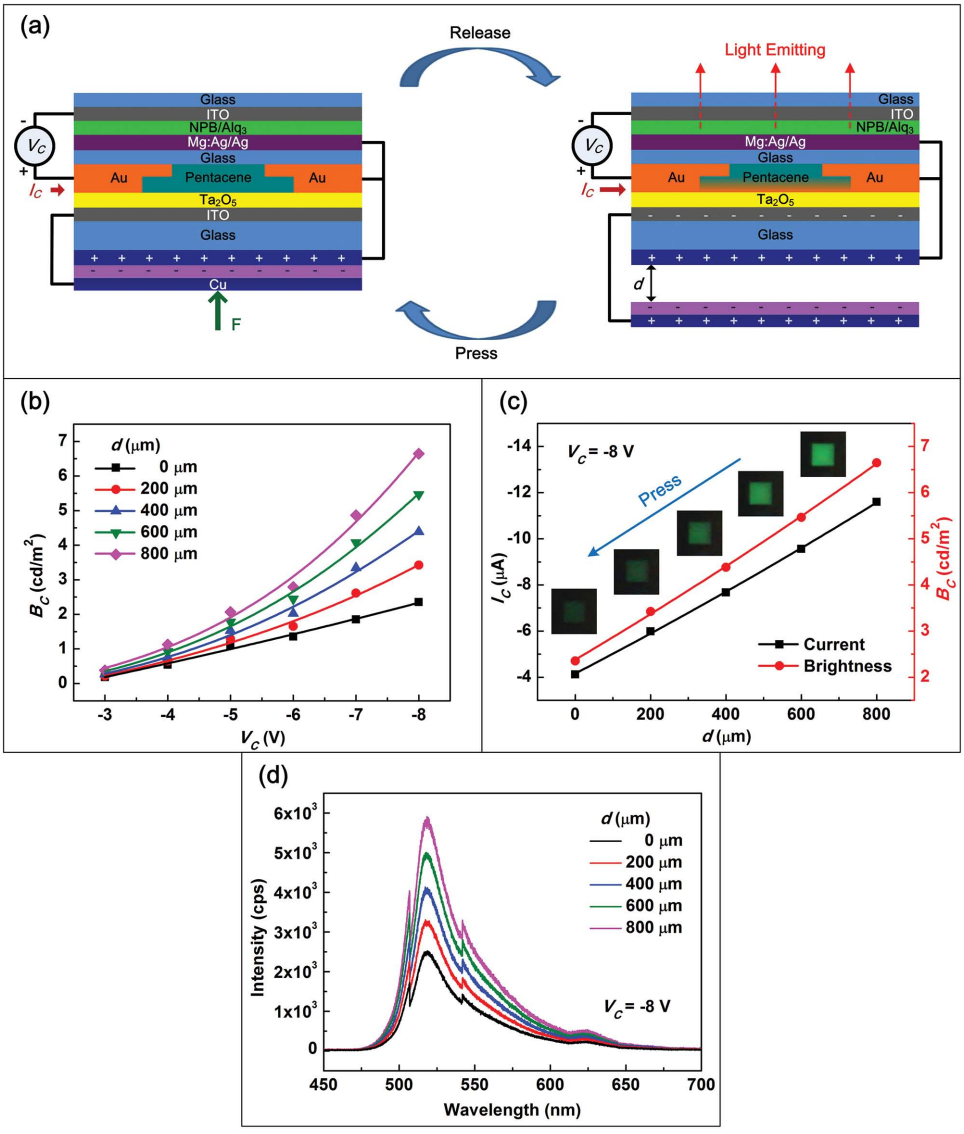


**Figure 5.** Principle and characteristics of the CG-LED in the first mode. a) Schematic working principle of the CG-LED. The brightness is increased when the gap distance *d* is increased. b) Brightness versus supply voltage of the CG-LED at different gap distances between the two frictional layers of the TENG. c) Current and brightness transfer characteristics with the change of the gap distance at a supply voltage of –8 V. The insets are the corresponding light-emitting photographs of the CG-LED at different gap distances. The CG-LED can turn from bright to dark when physically pressed. d) Corresponding optical spectrums of the CG-LED at different gap distances.

connected in series with a voltage source, and the drain current $I_C$ of the OTT is also the working current of the OLED. A spring damping system is designed for the CG-LED as shown in Figure S1 (Supporting Information). When the external force is applied to the CG-LED and the two frictional layers contact with each other, the drain current is lowered for the narrowed conduction channel, which makes the light emission very weak. While when the external force is released and the two frictional layers separate from each other at a certain distance, the drain current increases with the broadening conduction channel, which makes the light emission significantly enhanced. When the external force is applied again, the drain current turns back to low and the light emission is weakened to the original state. Therefore, the working current can be controlled by modulating the gap distance *d* between the two frictional layers and the light emission of the CG-LED can be gated by the external physical contact, which has the same effect as the traditional gate voltage in the OLETs.

The gap distance *d* in the CG-LED is also controlled and measured by the precise positioning system. Figure 5b shows the brightness versus supply voltage of the CG-LED at different gap distances *d* from 0 to 800 μm, and Figure 5c shows the working current and brightness transfer characteristics with the change of the distance *d* at a supply voltage of –8 V. The experimental results indicate that the brightness is increased with the increasing distance, which is in accordance with the working principle in Figure 5a. At a supply voltage of –8 V, the reverse working current increases from 4.1 to 11.6 μA

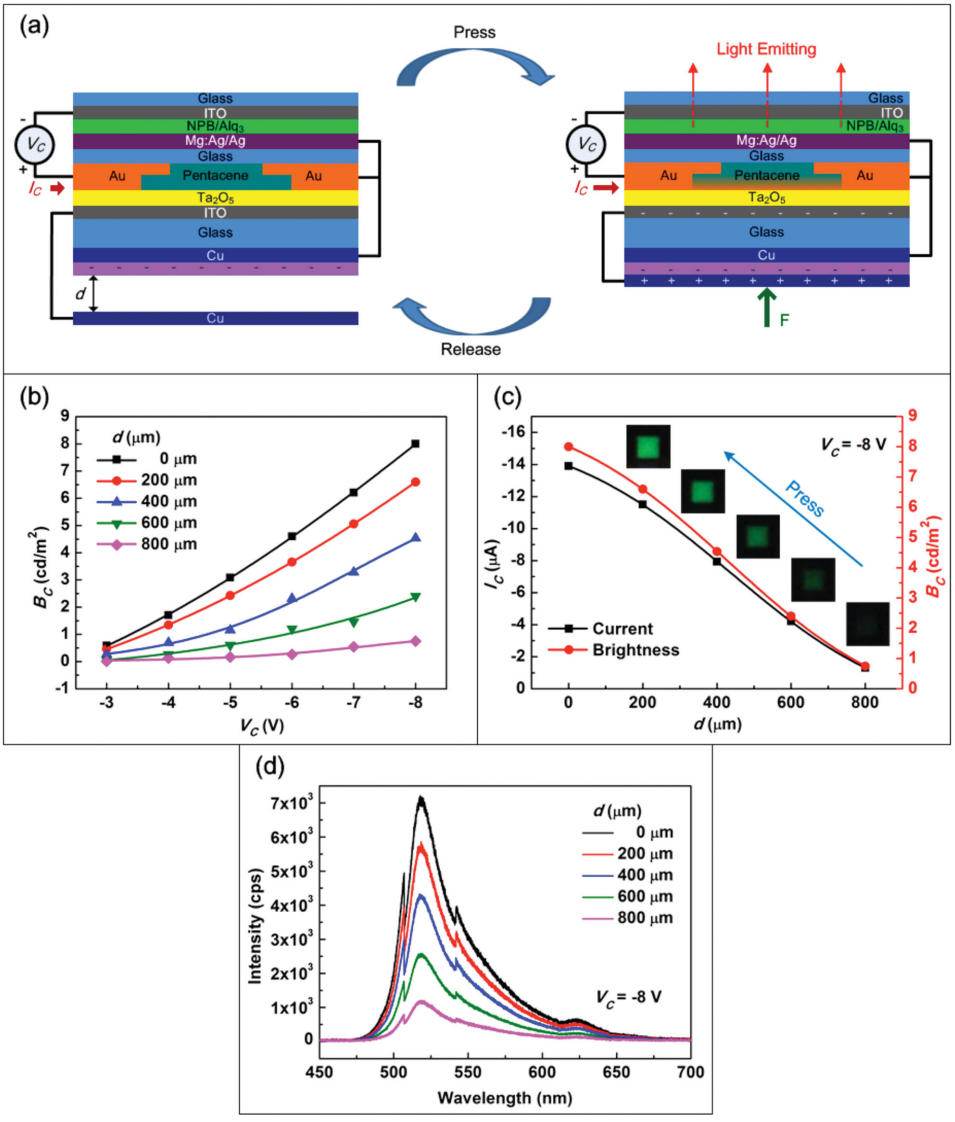


**Figure 6.** Principle and characteristics of the CG-LED in the second mode. a) Schematic working principle of the CG-LED. The brightness is increased when the gap distance *d* is decreased. b) Brightness versus supply voltage of the CG-LED at different gap distances between the two frictional layers of the TENG. c) Current and brightness transfer characteristics with the change of the gap distance at a supply voltage of −8 V. The insets are the corresponding light-emitting photographs of the CG-LED at different gap distances. The CG-LED can turn from dark to bright when physically pressed. d) Corresponding optical spectrums of the CG-LED at different gap distances.

and the brightness increases from 2.36 to 6.65 cd $m^{-2}$, which are both nearly linear to the increasing distance from 0 to 800 μm. The insets of Figure 5c are the corresponding light-emitting photographs of the CG-LED at the different gap distances, which demonstrates the CG-LED can turn from bright to dark when physically pressed. Figure 5d also shows the corresponding optical spectrums of the CG-LED at different gap distances for the light-emission transfer characteristics. Therefore, the CG-LED has successfully realized the modulated electroluminescence by the external force–induced contact electrification and established the direct interaction between the external environment and the electroluminescence device.

The other mode of the CG-LED is developed as well, and the working principle is schematically illustrated in **Figure 6**a. Different from the structure in the first mode, the PVC film is attached to the back side of the fixed Cu film and the surface has initial negative charges by triboelectrification. The mobile layer is only a piece of Cu film without any initial charges, which can vertically contact with and separate from each other by the external force. In the original state, the mobile layer is separated from the PVC film with a certain distance and the gate voltage of the OTFT is zero at this moment. When the external force is applied and the mobile layer contacts with the PVC film, the negative charges on the PVC film induce the electrons flow from the mobile Cu electrode to the ITO gate electrode for the

electrostatic induction. Due to the source electrode is connected to the fixed Cu film without any charges, a negative gate voltage is applied on the OTFT and the p-type conduction channel can be broadened, which will increase the drain current and thus enhance the light emission. While when the external force is released and the mobile Cu film separates from the PVC film to a certain distance, the balance of the induced charges causes the electrons to flow back from the ITO gate electrode to the mobile Cu film. The gate voltage turns back to zero and the conduction channel is narrowed, which will decrease the drain current and thus the light-emission intensity to the original state. Therefore, the working current and the light emission of the CG-LED can also be controlled by modulating the gap distance $d$ in this mode. This is the fundamental principle of the CG-LED.

The characteristics of the CG-LED in the second mode are investigated as well. The brightness versus supply voltage at different gap distances $d$ are shown in Figure 6b, and the working current and brightness transfer characteristics with the change of the distance $d$ at a supply voltage of −8 V are shown in Figure 6c. The experimental results indicate that the brightness is decreased with the increasing distance, which is in accordance with the working principle in Figure 6a. At a supply voltage of −8 V, the reverse working current decreases from 13.9 to 1.3 μA, and the brightness decreases from 8.01 to 0.75 cd $m^{-2}$, which are both nearly linear to the increasing distance from 0 to 800 μm. The insets of Figure 6c,d are the corresponding light-emitting photographs and optical spectrums at the different gap distances, respectively, which demonstrates the CG-LED in this mode can turn from dark to bright when physically pressed. Therefore, the light emission of the CG-LED in this mode can also be gated by the external force–induced contact electrification, which has the same modulation method but the reverse trend with the first mode.

## 3. Conclusion

In summary, by coupling an OTFT and a TENG in vertical contact-separation mode, an OTT has been proposed, in which the external physical contact can replace the traditional gate voltage, and the charge carrier transportation in the OTFT can be modulated by the contact-induced electrostatic potential of the TENG. By further coupling with an OLED, a CG-LED has been fabricated for the modulated electroluminescence, in which the operating current and light-emission intensity can be tuned/controlled by the external force–induced contact electrification. Two different modes of the CG-LED have been demonstrated and the brightness can be decreased and increased by the applied physical contact, respectively. Different from the conventional OLET controlled by an electrical signal, the CG-LED has realized the direct interaction between the external environment/stimuli and the electroluminescence device. The CG-LED is a new tribotronic device with only metal and organic functional materials, which has demonstrated the material variety for tribotronics. By introducing optoelectronics into tribotronics, the CG-LED has opened up a new field of tribophototronics and may have great prospects in interactive display, mechanical imaging, micro-opto-electro-mechanical systems, and flexible/touch optoelectronics.

## Supporting Information

Supporting Information is available from the Wiley Online Library or from the author.

## Acknowledgements

C.Z., J.L., and C.B.H. contributed equally to this work. The project was supported by National Natural Science Foundation of China (Grant Nos. 51475099 and 51432005), the "thousands talents" program for the pioneer researcher and his innovation team, China, and the Youth Innovation Promotion Association, CAS. The authors also thank Chaoying Zhang for her assistance in the SEM images analysis.

Received: June 15, 2015
Revised: July 9, 2015
Published online: August 4, 2015

[1] A. Hepp, H. Heil, W. Weise, M. Ahles, R. Schmechel, H. von Seggern, *Phys. Rev. Lett.* **2003**, *91*, 157406.
[2] M. Muccini, *Nat. Mater.* **2006**, *5*, 605.
[3] J. Clark, G. Lanzani, *Nat. Photonics* **2010**, *4*, 438.
[4] M. A. McCarthy, B. Liu, E. P. Donoghue, I. Kravchenko, D. Y. Kim, F. So, A. G. Rinzler, *Science* **2011**, *332*, 570.
[5] R. Haitz, J. Y. Tsao, *Phys. Status Solidi A* **2011**, *208*, 17.
[6] M. A. Baldo, R. J. Holmes, S. R. Forrest, *Phys. Rev. B* **2002**, *66*, 035321.
[7] C. Pan, L. Dong, G. Zhu, S. Niu, R. Yu, Q. Yang, Y. Liu, Z. L. Wang, *Nat. Photonics* **2013**, *7*, 752.
[8] R. Bao, C. Wang, L. Dong, R. Yu, K. Zhao, Z. L. Wang, C. Pan, *Adv. Funct. Mater.* **2015**, *25*, 2884.
[9] Q. Yang, Y. Liu, C. Pan, J. Chen, X. Wen, Z. L. Wang, *Nano Lett.* **2013**, *13*, 607.
[10] Y. Hu, Y. Zhang, L. Lin, Y. Ding, G. Zhu, Z. L. Wang, *Nano Lett.* **2012**, *12*, 3851.
[11] Y. Hu, Y. Chang, P. Fei, R. L. Snyder, Z. L. Wang, *ACS Nano* **2010**, *4*, 1234.
[12] Z. L. Wang, *J. Phys. Chem. Lett.* **2010**, *1*, 1388.
[13] Z. L. Wang, *Adv. Mater.* **2007**, *19*, 889.
[14] J. Zhou, Y. D. Gu, P. Fei, W. J. Mai, Y. F. Gao, R. S. Yang, G. Bao, Z. L. Wang, *Nano Lett.* **2008**, *8*, 3035.
[15] F. R. Fan, Z. Q. Tian, Z. L. Wang, *Nano Energy* **2012**, *1*, 328.
[16] Z. L. Wang, *Faraday Discuss.* **2014**, *176*, 447.
[17] C. Zhang, W. Tang, C. B. Han, F. R. Fan, Z. L. Wang, *Adv. Mater.* **2014**, *26*, 3580.
[18] C. Zhang, T. Zhou, W. Tang, C. B. Han, L. M. Zhang, Z. L. Wang, *Adv. Energy Mater.* **2014**, *4*, 1301798.
[19] S. Kim, M. K. Gupta, K. Y. Lee, A. Sohn, T. Y. Kim, K. S. Shin, D. Kim, S. K. Kim, K. H. Lee, H. J. Shin, D. W. Kim, S. W. Kim, *Adv. Mater.* **2014**, *26*, 3918.
[20] T. Zhou, C. Zhang, C. B. Han, F. R. Fan, W. Tang, Z. L. Wang, *ACS Appl. Mater. Interfaces* **2014**, *6*, 14695.
[21] X. S. Zhang, M. D. Han, R. X. Wang, F. Y. Zhu, Z. H. Li, W. Wang, H. X. Zhang, *Nano Lett.* **2013**, *13*, 1168.
[22] J. Chen, J. Yang, Z. Li, X. Fan, Y. Zi, Q. Jing, H. Guo, Z. Wen, K. C. Pradel, S. Niu, Z. L. Wang, *ACS Nano* **2015**, *9*, 3324.
[23] Z. H. Lin, G. Cheng, S. Lee, K. C. Pradel, Z. L. Wang, *Adv. Mater.* **2014**, *26*, 4690.
[24] W. Tang, T. Zhou, C. Zhang, F. R. Fan, C. B. Han, Z. L. Wang, *Nanotechnology* **2014**, *25*, 225402.

[25] C. B. Han, C. Zhang, W. Tang, X. H. Li, Z. L. Wang, *Nano Res.* **2014**, *8*, 722.
[26] C. Zhang, W. Tang, Y. K. Pang, C. B. Han, Z. L. Wang, *Adv. Mater.* **2015**, *27*, 719.
[27] C. B. Han, C. Zhang, J. J. Tian, X. H. Li, L. M. Zhang, Z. Li, Z. L. Wang, *Nano Res.* **2014**, *8*, 219.
[28] X. Y. Chen, M. Iwamoto, Z. Shi, L. M. Zhang, Z. L. Wang, *Adv. Funct. Mater.* **2014**, *25*, 739.
[29] C. Zhang, W. Tang, L. M. Zhang, C. B. Han, Z. L. Wang, *ACS Nano* **2014**, *8*, 8702.
[30] C. Zhang, L. M. Zhang, W. Tang, C. B. Han, Z. L. Wang, *Adv. Mater.* **2015**, *27*, 3533.
[31] X. H. Liu, G. F. Dong, D. Zhao, Y. P. Wang, L. Duan, L. D. Wang, Y. Qiu, *Org. Electron.* **2012**, *13*, 2917.
[32] Y. Liang, G. F. Dong, Y. Hu, L. D. Wang, Y. Qiu, *Appl. Phys. Lett.* **2005**, *86*, 132101.